SCIE 101: Scientific Research: Process and Presentation
Professors Maria Moreno, Kenneth Nelson, & Kallasnath Purushothaman

By submitting this essay, I attest that it is my own work, completed in accordance with University regulations. —Hannah Alpert

Determining the Ages, Metallicities, and Star Formation Rates of Brightest Cluster Galaxies

by Hannah Alpert[1], Louise Edwards[2]

[1]Science, Technology, and Research Scholar, Yale College, New Haven, CT, 06520
[2]Department of Astronomy, Yale University, New Haven, CT 06520

Abstract

Brightest cluster galaxies (BCGs), the most massive and luminous galaxies in the Universe, are elliptical galaxies located at the center of galaxy clusters. BCGs are composed of multiple stellar populations, each of which is characterized by its age, metallicity, and star formation rate. The method of BCG formation is unknown; our objective was to learn how BCGs formed and evolve. The spectral data from the stellar populations throughout four BCGs was gathered, reduced, and analyzed to determine their ages and metallicities, as well as their star formation rates and interactions with smaller galaxies. Because the absorption features of a spectrum reveal the compositions of the stars in the population, the equivalent widths of strong absorption lines were measured and compared to one another throughout different regions of each galaxy to determine how the stellar populations differ within the BCG. The relationship between the equivalent widths of the Na D and Mg b lines specifically revealed evidence of different star forming histories throughout each BCG. In particular, we determined that there were more recent star formation episodes in the center of many of the BCGs with older stellar populations in the outer regions of the galaxies. The next step of the process is to determine numerical ages and metallicities for the regions of the BCGs, and from these results it will be possible to determine how these most massive galaxies formed.

Introduction

Brightest cluster galaxies (BCGs) are the largest and most luminous galaxies in the Universe. They are usually elliptical galaxies found at the center of galaxy clusters and are

dominated by low-mass stars. BCGs are comprised of multiple populations of stars that are characterized by their age, metallicity, and rate of star formation. There are two main hypotheses for how BCGs formed: monolithic collapse and hierarchical building[1]. Under the monolithic collapse model, the stars in the BCG formed all together, so the ages and metallicites of the stellar populations across the galaxy are relatively uniform. Meanwhile, according the hierarchical building model, the galaxy built up through a number of smaller galaxies merging together. In this model, the different regions of the galaxies have varying ages and metallicities, since they formed in different parts of the Universe at different times.

Metallicity is a measure of the amount of heavy elements compared to the amount of Hydrogen in a gaseous body. Only massive stars produce the heavy elements; high- mass stars burn Hydrogen into Helium, Helium into Carbon and Oxygen, and Carbon and Oxygen into heavier and heavier elements until the stars explode as Type II supernova[2]. Upon explosion, the stars release into space all the elements they have created, and new stars form out of that enriched material, giving them a higher metallicity than the previous generation. High-mass stars release heavy elements like Magnesium after they die, while low-mass stars do not. Massive stars have a short lifetime of just 10 million years, so if stellar populations are observed that contain Magnesium in their atmospheres, this is a sign that high-mass stars have previously existed in that region of the Universe. Because of the brief lifetime of massive stars, the main component of BCGs today is low-mass stars that are rich in Sodium. Some stellar populations of low-mass stars are also rich in Magnesium, depending on if supernova have gone off in that area of the Universe. Studying the variation between the amount of absorption of Sodium and Magnesium in a stellar population reveals the characteristics of the different stellar populations throughout the galaxy.

To study this absorption, the spectra of the stars that make up the galaxy were examined.

The spectra of stars reveal what elements exist in the atmosphere of the star, indicating the properties of the gas at the time the star was born, not the composition of the interior of the star. Measuring the equivalent widths of the Na D and Mg b absorption lines gives a measure of the amount of absorption of these two elements. The relative differences between these two lines indicate the properties of the stellar populations that are in the galaxy[3]. The purpose of the project is to visualize the emission line regions and use the equivalent widths of the absorption lines to determine the ages and metallicites of the different regions throughout the BCGs, working to determine how these galaxies formed and evolved.

In this study, spectral data were collected for four BCGs in low redshift clusters across a large field centered on the BCG of interest using the Sparsepak[4] instrument on the 3.5-meter WIYN Telescope. The data was reduced into spectra that could be analyzed and the Lick indices[5], similar to the equivalent widths, of the absorption lines could be calculated. The variation between the amount of Sodium and Magnesium absorption was then studied across the BCG, so far for the case of A1795, so that the stellar populations could be differentiated from one another.

Materials and Methods

Data Collection

Brightest cluster galaxies (BCGs) A1795, Z2844, MKW3, and A1668 were observed over the span of three nights between April 30 and May 3, 2013 using the Sparsepak instrument on the 3.5-meter WIYN Telescope. Sparsepak[4] is a spectrograph with 82 optical fibers of which 75 are arranged in a grid of dimensions 72" x 71.3" with a tightly packed center, and 7 are sky fibers located on the outside of two of the sides of the grid (See Figure 1). Two additional offsets were applied to fully integrate the central regions. The first offset was 0" East, 5.6" South from the original position and the second was 4.9" West, 2.8" North from the original position, which are

the standard dithers for Sparsepak. Due to weather conditions and a manual telescope error, A1668 was only observed at two positions, and A1795 was observed at four positions. Each fiber produced a spectrum from the region covered. The spectrograph gathered wavelengths between about 4000Å and 7000Å, and the GG-420 filter was used to cut second order lines.

Before observing the BCGs each night, a set of ten 4-second dome flats, ten 5- second arcs, ten biases, ten 4-second darks, and ten 300-second darks were captured. Flats are exposures taken with a light on and the dome covered to show defects of the CCD or other lighting problems; arcs, or comparison lamps, are taken for wavelength calibration purposes; biases are zero second exposures that show the noise of the camera; and darks are taken with no light and the dome closed to reveal problems like "hot pixels," or pixels with high leakage. At the end of each night, another set of ten biases and ten 300-second darks were taken as well. On the first night of the observing run, A1795 was observed in its home position and the first offset position and Z2844 was observed in the home position and the two offsets. On the second night, the observations of A1795 and Z2844 were completed, and MKW3 observations were done fully as well. On the third night, A1668 was observed in the home position and at one offset (see Table 1).

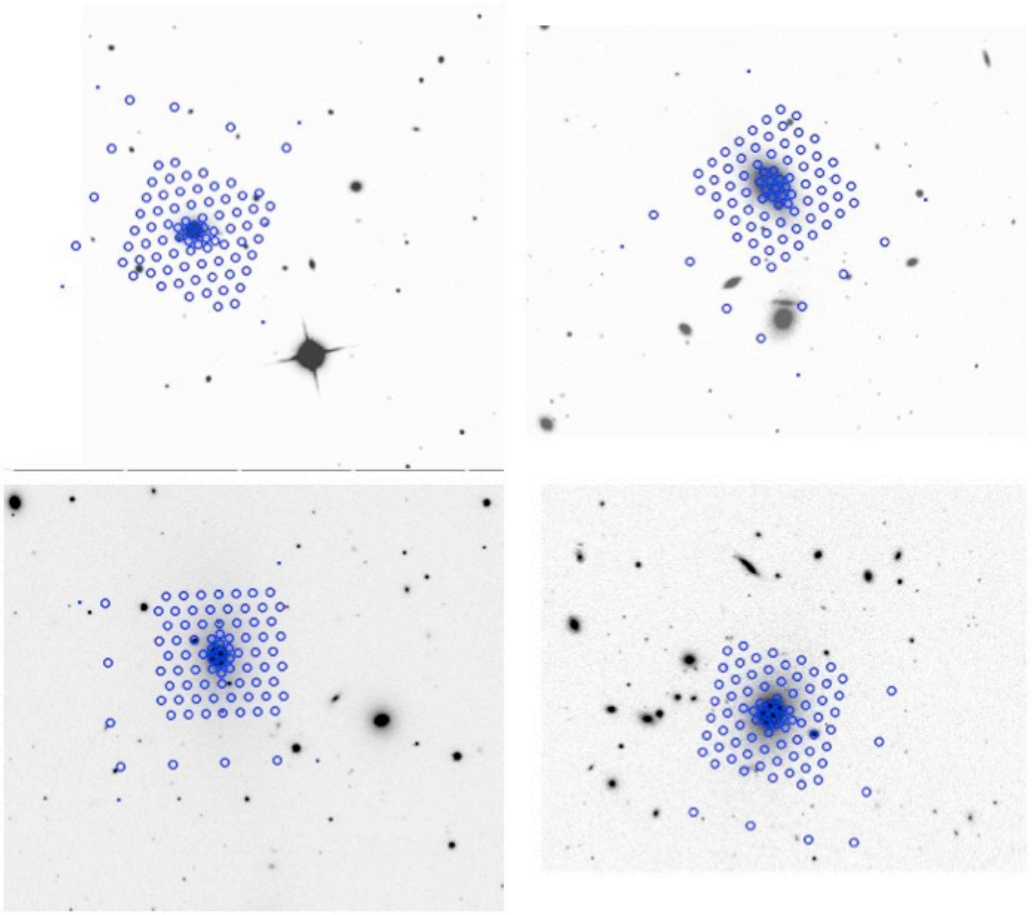

Figure 1. *Inverted color images of the four galaxies observed overlaid with the grid design of the Sparsepak fibers. Top row from left to right: A1795, Z2844. Bottom row from left to right: MKW3, A1668.*

Table 1. *Observational Data*

Object Name	Right Ascension (h:m:s)	Declination (h:m:s)	Total I Time (sec)	Rot. Pos. Offset Angle (deg.)
A1795 Home	13:48:51.877	+26:35:35.952	3600	107.6°
A1795 Offset1a	Home+2.8"W	Home+5.6"S	3600	107.6°
A1795 Offset1b	Home+4.9"E	Home+5.6"S	1800	107.6°
A1795 Offset2	Home+4.9"W	Home+2.8"S	3600	107.6°
Z2844 Home	10:02:36.51	+32:42:22.87	1800	65.6°
Z2844 Offset1	Home+0"	Home+5.6"S	1800	65.6°
Z2844 Offset2	Home+4.9"W	Home+2.8"S	1800	65.6°
MKW3 Home	15:21:51.48	+07:42:35.614	3600	90.6°
MKW3 Offset1	Home+0"	Home+5.6"S	1800	90.6°
MKW3 Offset2	Home+4.9"W	Home+2.8"S	900	90.6°
A1668 Home	13:04:03.589	+19:16:16.842	3600	95.6°
A1668 Offset1	Home+0"	Home+5.6"S	1800	95.6°

Data Reduction

Pre-processing

The data was reduced using the Image Reduction and Analysis Facility (IRAF) V2.14, specifically the *dohydra* package. The images were trimmed then separated based on their positions. For each night, the bias exposures and the twenty 300-second dark exposures were each median-combined and then subtracted respectively from the data. Similarly, a median flat field was constructed. Finally, every group of exposures at each position was median-combined.

The program L.A. Cosmic[6] was used to remove some of the cosmic rays that were present throughout the data. The output of L.A. Cosmic was a new spectrum with many cosmic rays removed and a bad pixel mask. Finally, *dohydra* was run over the target files for each position to actually apply the flat field correction, which corrected the images for differences in sensitivity between pixels and optical distortions that may have existed.

Sky Subtraction

In our sample, the emission and absorption lines of the BCGs are faint, so it was important to remove the skylines carefully. The first method we tested for sky subtractionwas using exposures of separate sky fields and subtracting the sky spectrum of each aperture from the galaxy spectrum of the same aperture. However, this resulted in poor sky subtractions, so instead the spectra from the six sky apertures[4] were copied for every group at each position and then these apertures were median-combined together. The median sky spectrum was subtracted from the object spectra for each group of exposures, allowing the sky spectrum to be subtracted from all 82 of the apertures. The sky was subtracted from the data from each of the three nights separately, and then all of the groups at each position were median-combined together so that there were singular sky- subtracted files for the home and offset positions for each BCG. Finally, the remaining cosmic rays were manually removed using the editing tools in *splot*, the IRAF package that displayed the

spectra.

Data Analysis

Lick Indices and Equivalent Width Measurement

The equivalent widths of the absorption and emission lines were measured in order to determine characteristics of the galaxies. The *deredden* feature was used to correct the spectra in order to account for dust extinction based on the E(B-V) values of the galaxies. The spectra were also shifted based on the galaxies' redshift values using the *dopcor* feature. To describe the line absorption, Lick indices[5] were measured using the LECTOR[7] program. The Lick index of an absorption line is the measurement of the flux between two wavelength values scaled to the continuum level, and LECTOR returned this measurement for each of 32 absorption features, as well as their errors. The signal-to-noise ratio (SNR) of each absorption line could be calculated by dividing the Lick index value by the error. Meanwhile, to measure the emission lines, we modeled the peaks with de-blended Gaussian profiles, which returned the center, flux, equivalent width, and Gaussian full width half max of each peak. While measurements of 32 Lick indices were gathered, results are presented for the Na D, Mg b, and Hβ lines, which were analyzed in more detail, as each of these lines is instrumental in determining the metallicity and age of a stellar population within a galaxy[8].

Results: Case of A1795

Visualization of Galaxies: Emission Lines

Images of the BCGs were created to visualize the emission features of the galaxies in different wavelengths. The color of the image is correlated with the brightness of the aperture in the specified wavelength region. A map of each galaxy was made over the entire range of wavelengths collected and then specific wavelength regions were chosen, including the region associated with Hα, which is around 6900Å before redshift correction. Figure 2 shows an example of the images

created for A1795. These images indicated that the center of the galaxy was the brightest in all wavelengths, but there were certain patterns of emission in the Hα that suggested a tail of star formation outwards from the center. There were also some abnormally bright apertures; the one in the bottom left corner of Figure 2 indicates a smaller galaxy possibly interacting with the BCG.

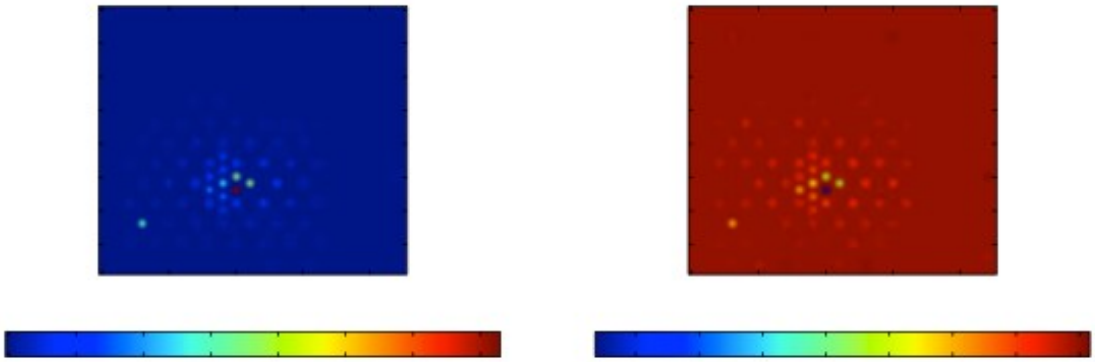

Figure 2*. Images of A1795. From left to right: the full continuum and the continuum subtracted flux between 6850 and 6940 Å, which is the Hα region.*

Graphical Analysis of Equivalent Widths of Absorption Features

The metallicities and ages of stellar populations are determined by comparing the equivalent widths of certain absorption lines, including Na D, Mg b, and Hβ. For each absorption line, SNR was plotted against the distance from that aperture to the center of the galaxy. Likewise, the equivalent widths of the lines were graphed against the distance to the center (see example in Figure 3). The SNR was determined by dividing the equivalent width of the line by the error value provided by the LECTOR program. The horizontal line on the SNR graphs is at SNR=3 because that is a standard accepted SNR for reliable data[9]. Because the points begin to be below the SNR=3 line at a distance of 10" from the center, a vertical line was drawn there on the equivalent width graphs.

The graphs in Figure 3 show that the SNR of Na D and Mg b is very high near the center of

the BCG, which is where the absorption in expected to be the strongest with the least noise. However, the SNR for the Hβ absorption is quite low throughout each of the BCGs. In the Hβ graph of A1795 there are a small number of high-SNR points but they are not in the center of the galaxy, possibly because the Hβ absorption is polluted by strong Hα emission in the center of the galaxy. The points that have high SNRs in this graph may either represent small, bright galaxies in the same field of view as A1795 or correspond to areas where the Hα emission strongly overpowers the Hβ absorption.

The SNRs of Mg b and Na D were plotted against each other, as were the equivalent widths of the two lines (example in Figure 4). The Mg b vs. Na D SNR graphs show clearly that as the SNR of Mg b increases, so does the SNR of Na D for all of the BCGs. These graphs also show that the points closer to the center of the galaxy have
much higher SNRs. This trend indicates that there is stronger emission and absorption in the center of the galaxies than in the outer regions, with relatively little noise.

The graphs of the equivalent widths of Mg b and Na D for each BCG reveal that the apertures that are various distances from the center of the galaxy tend to cluster in different regions on the graph depending on this distance. The general trend of these graphs indicates that the points corresponding to the apertures close to the center of the galaxy group together slightly to the right and above the points representing the apertures further out from the center. This suggests different ages and metallicities for each of these regions of the galaxy. Stronger Mg b absorption lines have greater equivalent widths, and an increase in equivalent width corresponds to an increase in time; prominent Mg b lines suggest that many generations of massive stars have had the chance to live and die in that region of the galaxy. Similarly, the equivalent width of the Na D line also grows with an increase in time because Na D absorption is proportional to the number of low-mass stars

in the area. Low-mass stars live for a long time and die out very slowly, so old low-mass stars continue to exist as more are formed. The clustering of the blue points above and to the right of the magenta ones in Figure 4b implies that the center of the galaxy is made out of younger stars than the outer region of the galaxy, suggesting recent star formation episodes in the central region of the BCG. The points corresponding to the apertures even further out than 10″, however, seem to be spread randomly, likely because the data past 10″ is too noisy to be accountable.

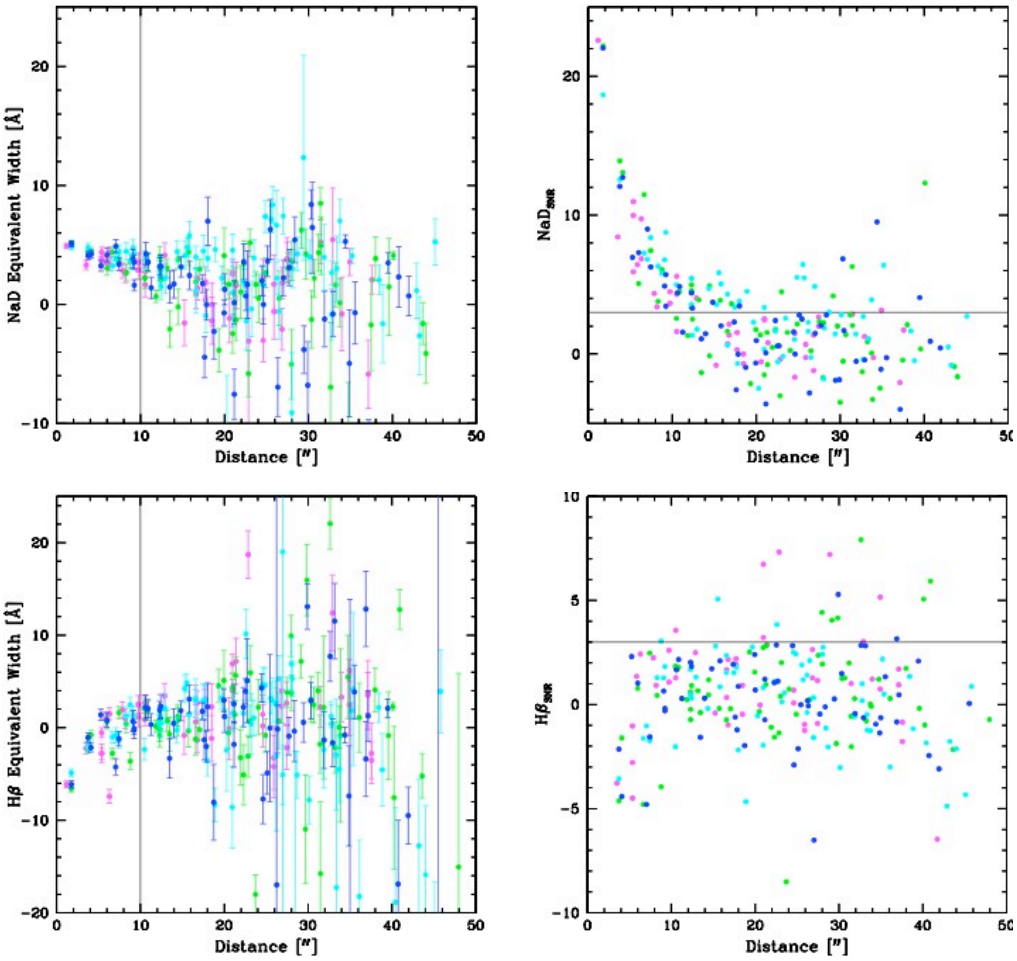

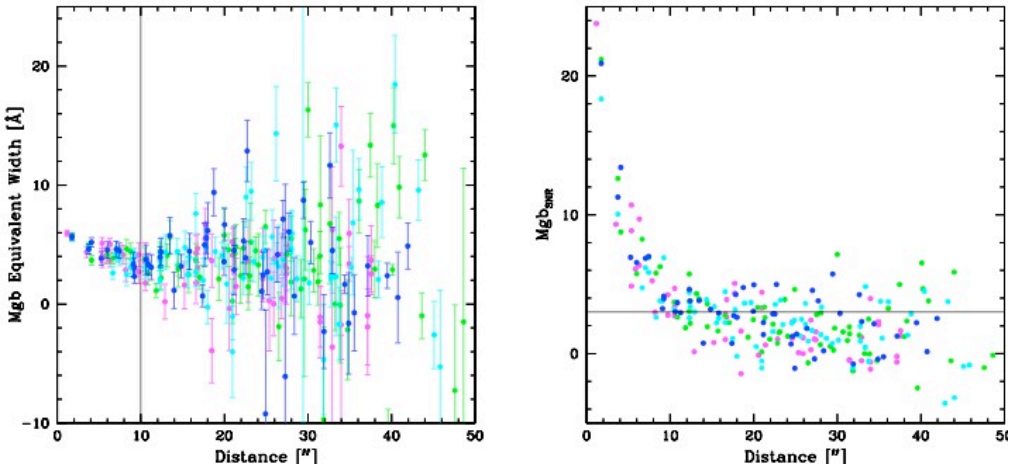

Figure 3. *Graphs of emission features of A1795. Columns: From left to right, equivalent widths with error bars, signal-to-noise ratios. Rows: From top to bottom, Na D, Hβ, Mg b. Colors: Home position is represented by magenta points, Offset 1A by green, Offset 1B by cyan, and Offset 2 by blue. In the graphs of SNR vs. distance from center of galaxy, the horizontal line is at SNR=3. The vertical line on the graphs of equivalent width vs. distance is at distance=10″. The location of this line was set based on the SNR graphs, which show that the points begin to fall below the SNR=3 line at about 10″.*

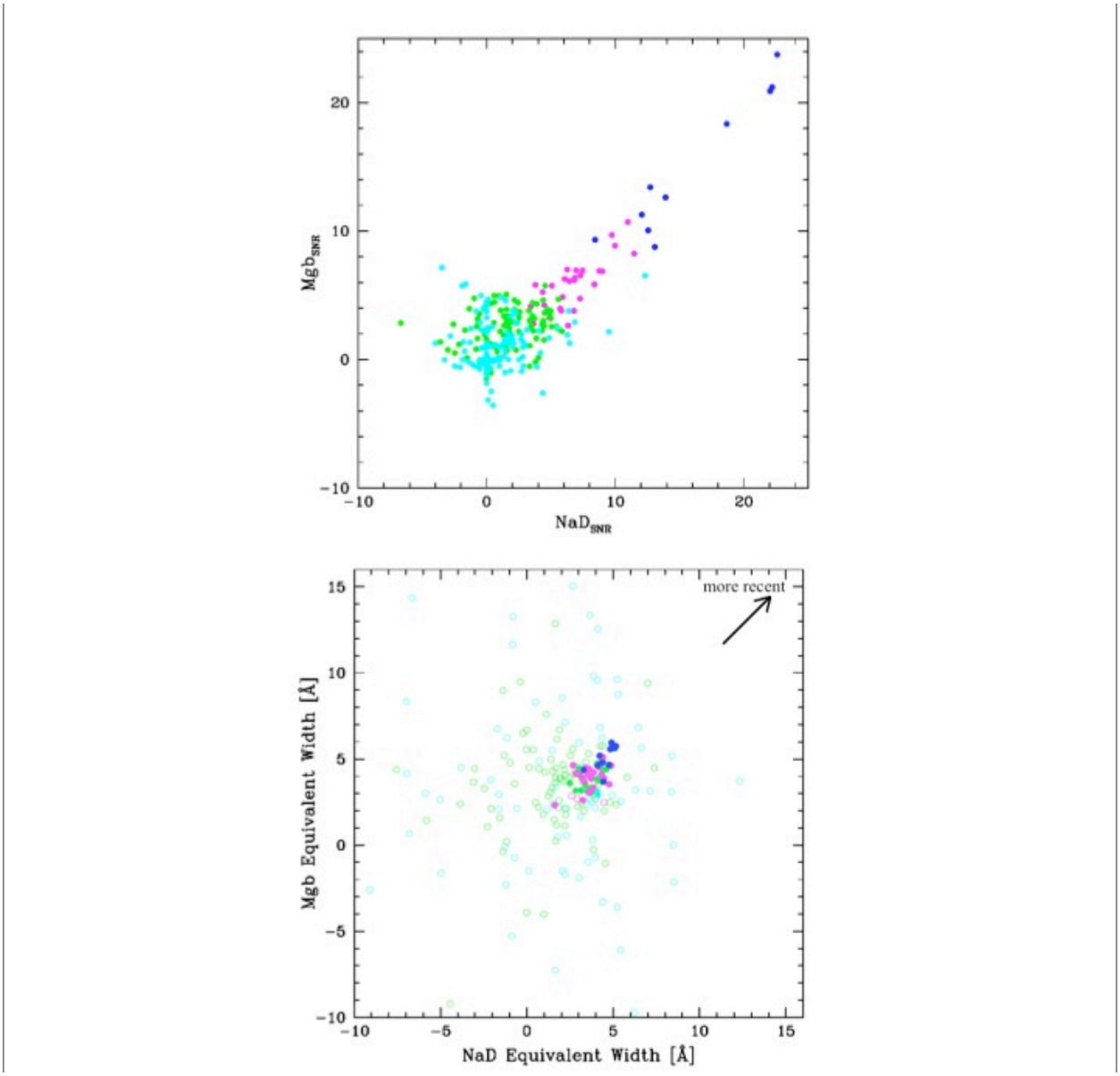

Figure 4. *Graphs of Mg b vs. Na D for A1795. (a) Top: Signal-to-noise ratios. Blue dots represent the apertures that are within 5" from the center of the galaxy, magenta is from 5" to 10", green is from 10" to 25' and cyan is greater than 25". (b) Bottom: Equivalent widths. Colors are same as above. Open circles represent points that have an SNR less than 3, solid circles represent points that have an SNR greater than 3.*

Discussion

Visualization of Galaxies: Emission Lines

The visualization of the galaxies revealed interactions with smaller galaxies and regions of high emission in the Hα region of the spectrum, which denote star formation. Figure 2 indicates the presence of a small, bright galaxy in the field of view of A1795. Other images showed potential tails of Hα emission outside the center of the BCG, implying that there may be star formation occurring in other parts of the galaxy that are not as bright in the visual wavelengths. To complete the analysis of these visualizations, the galaxies will have to be visualized over different parts of the spectrum. Other emission lines, like NII, SII, and Hβ, can provide information about the stellar population's metallicity.

We can also compare the emission features of the BCGs to the ages and metallicities of the stellar populations that we determine from the absorption features and confirm that these results correspond with one another. For example, because Figure 4b indicated recent star formation episodes in the center of the galaxy, we expect that the visualization of this BCG would show strong Hα emission in these same apertures. Agreement between these two sources would strongly suggest that the results are accurate and can be used for further analysis. These results can also be compared to similar studies performed on BCGs in different wavelength regions such as the x-ray and infrared parts of the spectrum[10,11], which examine emission in these wavelengths as a measure of star formation in galaxies.

Graphical Analysis of Equivalent Widths of Absorption Features

As expected, the SNR of both the Na D and Mg b lines are significantly higher near the center of the BCG, as shown in Figure 3, due to the high amount of absorption and little noise. The low SNR of Hβ absorption is reasonable as well, as Hβ absorption occurs in tandem with Hα

emission. Because the center of the galaxy is likely experiencing current or recent star formation, the Hβ absorption is polluted by this Hα emission; thus the Hβ absorption features are much less prominent and more noisy than they would be otherwise. Future analysis will include determining the correct Hβ values by subtracting out the Hα emission, which can be accomplished because there are known ratios between Hα emission and Hβ absorption. The amount of Hβ absorption is an important value because it is one of the most significant age indicators of a stellar population and will be used to make numerical age estimates[12].

The graph of equivalent widths of Mg b vs. Na D (Figure 4b) indicates that the different regions of the galaxy, based on their distance from the galactic center, have different ages and metallicites. The location of the blue points on the graph, to the right and above the magenta points, reveals more recent star formation episodes in the center of the BCG. The same graphs were created for each of the BCGs studied although the figures are only shown for A1795. However, the trend of recent star formation in the center of the BCG was followed for most of the BCGs we observed, suggesting that it is possibly a feature of most of these galaxies, but we cannot draw any conclusions until our sample size is increased. However, our determination of star formation in the center of the galaxy appears to be in agreement with other studies. An examination of 48 BCGs in X-ray luminous clusters revealed that in a number of the galaxies there was a trend of bluing towards the galactic center; this tendency was interpreted as corresponding to recent star formation in the central regions[13].

Further Analysis

The BCGs will be divided further into more regions, rather than just four regions based on the distance from the center of the galaxy. Closer comparisons of these regions will reveal how the ages and metallicities of the areas differ. Varying ages and metallicities of the different regions will

suggest that BCGs are likely created by smaller galaxies, each formed individually in time and space, interacting and merging together. Meanwhile, relatively uniform ages and metallicities of the stellar populations throughout the BCGs will indicate that the whole galaxy may have formed at the same time and location.

After qualitative analysis of the stellar populations in the BCGs has been performed, we will determine the numerical metallicities and ages of the different regions of the galaxies. A program called EZ_Ages[12], which matches the measurements of the Lick indices to various age and metallicity models, will be used. This program will reveal the differences in ages and types of stars throughout each BCG, and with this information we aim to determine how these galaxies formed.

Other future analysis involves matching the results of the ages of stellar populations to the location of emission lines because emission lines indicate actual star formation rates of young stellar population. The emission lines, unlike the absorption lines, come from high-mass stars instead of low-mass stars. We will measure the emission lines to calculate numerical star formation rates. With this information, we will determine which parts of the galaxy built up first, to reveal how these galaxies formed and evolved. BCGs are the brightest, most massive, and possibly the oldest galaxies in the Universe, so if we can determine their formation and evolution history, we will be able to make informed hypotheses about how the first galaxies in the Universe formed and how other types of galaxies form now.

Finally, five more nights of observations are planned for this coming November (2013). We hope to gather spectral data for more galaxies to give us a complete sample of all of the galaxies observationally available to us. We will reduce and analyze this data in the same way, which will allow us to draw more general conclusions about the formation and evolution of brightest cluster galaxies.

Strengths and Limitations

One limitation, inherent in observational astronomy, is the amount of data we were able to collect. Although we were allotted three nights to observe at Kitt Peak, on the first night the telescope was unusable for half of the night because of high winds, and on the third night the telescope was closed for most of the night because of an excessive amount of dust in the air. These problems limited the amount of exposure time for many of the objects. The wind also caused slight movement of the telescope, which may have inhibited the quality of the data.

Conclusion

The spectral data of four BCGs was examined to determine the qualitative variations in metallicity and age of the stellar populations within each of four galaxies. The equivalent widths of 32 absorption features were measured. The values of the equivalent widths of the Na D and Mg b absorption lines were particularly important in determining the metallicity of each stellar population, and therefore the history of star formation that has occurred in each region of the BCG. Comparing the equivalent widths of the Na D and Mg b lines in each aperture indicated that the stars in the center of the BCG A1795 are newer and younger, implying that episodes of star formation have occurred in the central regions of the galaxy more recently than in the outer regions. This trend appears to be present in most of the BCGs studied. Analysis of further divisions of the BCGs as well as the determination of numerical ages and metallicities of the stellar populations within the BCGs will reveal how these bright, massive galaxies formed.

Acknowledgments

This work was supported by the National Space Grant Consortium and the STARS Program at Yale. This study uses data gathered with Sparsepak on the WIYN Telescope at Kitt Peak National Observatory. We would like to thank Sean McGee for his assistance on the telescope proposal and the visualization code; instrument scientist Jenny Power and telescope

operators Krissy Reetz and Dave Summers for their valuable help in obtaining observations; and

Vasilije Dobrosavljevic for his help in fitting Gaussian profiles.

References

1. Collins, C.; Scott, J.; Hilton, M.; Kay, S.; Stanford, S.; Davidson, M.; Hosmer, M.; Hoyle, B.; Liddle, A,; Lloyd-Davies, E.; Mann, R.; Mehrtens, N.; Miller, C.; Nichol, R.; Romer, A.; Sahlén, M.; Viana, P.; West, M. Early assembly of the most massive galaxies. *Nature* **2009**, *458*, 603-606.
2. Massey, P. Massive Stars in the Local Group: Implications for Stellar Evolution and Star Formation. *Astron. Astrophys.* **2009**, *41*, 15-56.
3. Edwards, L.O.V.; Robert, C.; Mollá, M.; McGee, S. The diverse nature of optical emission lines in brightest cluster galaxies: IFU observations of the central kiloparsec. *Mon. Not. Roy. Astron. Soc.* **2009,** *396*(4), 1953-1971.
4. Bershady, M.; Andersen, D.; Harker, J.; Ramsey, L.; Verheijen, M. SparsePak: A Formatted Fiber Field Unit for the WIYN Telescope Bench Spectrograph. I. Design, Construction, and Calibration. *Pub. Astron. Soc. Pac.* **2004**, *116*(820): 565-590.
5. Thomas, D.; Maraston, C.; Bender, R.; Stellar population models of Lick indices with variable element abundance ratios. *Mon. Not. Roy. Astron. Soc.* **2003**, *339*(3), 897-911.
6. van Dokkum, P. G.; Cosmic-Ray Rejection by Laplacian Edge Detection. *Publ. Astron. Soc. Pac.* **2001,** *113*, 1420-1427.
7. Worthey, G.; Ottaviani, D.; H gamma and H delta Absorption Features in Stars and Stellar Populations. *Astrophys. J. Supp. Ser.* **1997**, *111*, 377-386.
8. Franchini, M.; Morossi, C.; Di Marcantonia, P.' Mlagini, M.; Chavez, M.; Rodriquez-Merino, L.; Synthetic Lick Indices and Detection of Enhanced Stars. *Astrophys. J.* **2004,** *601*, 485-499.
9. NDT Resource Center. Signal-to-Noise Ratio. http://www.ndt-ed.org/EducationResources/CommunityCollege/Ultrasonics/Physics/signaltonoise.htm (accessed Aug 3, 2013).
10. Stevens, J.; Ivison, R.; Dunlop, J.; Smail, I.; Percival, W.; Hughes, D.; Rottgering, H.; van Breugel, W.; Reuland, M.; The Formation of Cluster Elliptical Galaxies as Revealed by Extensive Star Formation. *Nature*. **2003**, *425*, 264-267.
11. O'Dea, P.; Baum, S.; Privon, G.; Noel-Storr, J.; Quillen, A.; Zufelt, N.; Park, J.; Edge, A.; Russell, H.; Fabian, A.; Donahue, M.; Sarazin, C.; McNamara, B.; Bregman, J.; Egami, E. An Infrared Survey of Brightest Cluster Galaxies. II. Why are Some Brightest Cluster Galaxies Forming Stars? *Astrophys. J.* **2008**, *681*(2), 1035-1045.
12. Graves, G.; Schiavon, R.; Measuring Ages and Elemental Abundances from UNresolved Stellar Populations: Fe, Mg, C, N, and Ca. *Astrophys. J.* **2008**, *177*, 446-464.
13. Bildfell, C.; Hoekstra, H.; Babul, A.; Mahdavi, A.; Resurrecting the Red from the Dead: Optical Properties of BCGs in X-ray Luminous Clusters. *Mon. Not. Roy. Astron. Soc.* **2008**, 1-20.